1-1995

Inclusive production of neutral vector mesons in hadronic Z decays

D. BUSKULIC

Manoj THULASIDAS

Singapore Management University, manojt@smu.edu.sg

EUROPEAN ORGANIZATION FOR NUCLEAR RESEARCH

CERN-PPE/95-100
6 July 1995

Inclusive Production of Neutral Vector Mesons in Hadronic Z Decays

The ALEPH Collaboration*

Abstract

Data on the inclusive production of the neutral vector mesons $\rho^0(770)$, $\omega(782)$, $K^{*0}(892)$, and $\phi(1020)$ in hadronic Z decays recorded with the ALEPH detector at LEP are presented and compared to Monte Carlo model predictions. Bose-Einstein effects are found to be important in extracting a reliable value for the ρ^0 production rate. An average ρ^0 multiplicity of 1.45 ± 0.21 per event is obtained. The ω is detected via its three pion decay mode $\omega \to \pi^+\pi^-\pi^0$ and has a total rate of 1.07 ± 0.14 per event. The multiplicity of the K^{*0} is 0.83 ± 0.09, whilst that of the ϕ is 0.122 ± 0.009, both measured using their charged decay modes. The measurements provide information on the relative production rates of vector and pseudoscalar mesons, as well as on the relative probabilities for the production of hadrons containing u, d, and s quarks.

(Submitted to Zeitschrift für Physik C)

*See next pages for the list of authors

The ALEPH Collaboration

D. Buskulic, D. Casper, I. De Bonis, D. Decamp, P. Ghez, C. Goy, J.-P. Lees, A. Lucotte, M.-N. Minard, P. Odier, B. Pietrzyk

Laboratoire de Physique des Particules (LAPP), IN^{2}P^3-CNRS, 74019 Annecy-le-Vieux Cedex, France

F. Ariztizabal, M. Chmeissani, J.M. Crespo, I. Efthymiopoulos, E. Fernandez, M. Fernandez-Bosman, V. Gaitan, Ll. Garrido,[15] M. Martinez, S. Orteu, A. Pacheco, C. Padilla, F. Palla, A. Pascual, J.A. Perlas, F. Sanchez, F. Teubert

Institut de Fisica d'Altes Energies, Universitat Autonoma de Barcelona, 08193 Bellaterra (Barcelona), Spain[7]

A. Colaleo, D. Creanza, M. de Palma, A. Farilla, G. Gelao, M. Girone, G. Iaselli, G. Maggi,[3] M. Maggi, N. Marinelli, S. Natali, S. Nuzzo, A. Ranieri, G. Raso, F. Romano, F. Ruggieri, G. Selvaggi, L. Silvestris, P. Tempesta, G. Zito

Dipartimento di Fisica, INFN Sezione di Bari, 70126 Bari, Italy

X. Huang, J. Lin, Q. Ouyang, T. Wang, Y. Xie, R. Xu, S. Xue, J. Zhang, L. Zhang, W. Zhao

Institute of High-Energy Physics, Academia Sinica, Beijing, The People's Republic of China[8]

G. Bonvicini, M. Cattaneo, P. Comas, P. Coyle, H. Drevermann, A. Engelhardt, R.W. Forty, M. Frank, R. Hagelberg, J. Harvey, R. Jacobsen,[24] P. Janot, B. Jost, J. Knobloch, I. Lehraus, C. Markou,[23] E.B. Martin, P. Mato, H. Meinhard, A. Minten, R. Miquel, T. Oest, P. Palazzi, J.R. Pater,[27] J.-F. Pusztaszeri, F. Ranjard, P. Rensing, L. Rolandi, D. Schlatter, M. Schmelling, O. Schneider, W. Tejessy, I.R. Tomalin, A. Venturi, H. Wachsmuth, W. Wiedenmann, T. Wildish, W. Witzeling, J. Wotschack

European Laboratory for Particle Physics (CERN), 1211 Geneva 23, Switzerland

Z. Ajaltouni, M. Bardadin-Otwinowska,[2] A. Barres, C. Boyer, A. Falvard, P. Gay, C. Guicheney, P. Henrard, J. Jousset, B. Michel, S. Monteil, J-C. Montret, D. Pallin, P. Perret, F. Podlyski, J. Proriol, J.-M. Rossignol, F. Saadi

Laboratoire de Physique Corpusculaire, Université Blaise Pascal, IN^{2}P^3-CNRS, Clermont-Ferrand, 63177 Aubière, France

T. Fearnley, J.B. Hansen, J.D. Hansen, J.R. Hansen, P.H. Hansen, B.S. Nilsson

Niels Bohr Institute, 2100 Copenhagen, Denmark[9]

A. Kyriakis, E. Simopoulou, I. Siotis, A. Vayaki, K. Zachariadou

Nuclear Research Center Demokritos (NRCD), Athens, Greece

A. Blondel,[21] G. Bonneaud, J.C. Brient, P. Bourdon, L. Passalacqua, A. Rougé, M. Rumpf, R. Tanaka, A. Valassi,[31] M. Verderi, H. Videau

Laboratoire de Physique Nucléaire et des Hautes Energies, Ecole Polytechnique, IN^{2}P^3-CNRS, 91128 Palaiseau Cedex, France

D.J. Candlin, M.I. Parsons

Department of Physics, University of Edinburgh, Edinburgh EH9 3JZ, United Kingdom[10]

E. Focardi, G. Parrini

Dipartimento di Fisica, Università di Firenze, INFN Sezione di Firenze, 50125 Firenze, Italy

M. Corden, M. Delfino,[12] C. Georgiopoulos, D.E. Jaffe

Supercomputer Computations Research Institute, Florida State University, Tallahassee, FL 32306-4052, USA [13,14]

A. Antonelli, G. Bencivenni, G. Bologna,[4] F. Bossi, P. Campana, G. Capon, V. Chiarella, G. Felici, P. Laurelli, G. Mannocchi,[5] F. Murtas, G.P. Murtas, M. Pepe-Altarelli

Laboratori Nazionali dell'INFN (LNF-INFN), 00044 Frascati, Italy

S.J. Dorris, A.W. Halley, I. ten Have,[6] I.G. Knowles, J.G. Lynch, W.T. Morton, V. O'Shea, C. Raine, P. Reeves, J.M. Scarr, K. Smith, M.G. Smith, A.S. Thompson, F. Thomson, S. Thorn, R.M. Turnbull

Department of Physics and Astronomy, University of Glasgow, Glasgow G12 8QQ,United Kingdom[10]

U. Becker, O. Braun, C. Geweniger, G. Graefe, P. Hanke, V. Hepp, E.E. Kluge, A. Putzer, B. Rensch, M. Schmidt, J. Sommer, H. Stenzel, K. Tittel, S. Werner, M. Wunsch

Institut für Hochenergiephysik, Universität Heidelberg, 69120 Heidelberg, Fed. Rep. of Germany[16]

R. Beuselinck, D.M. Binnie, W. Cameron, D.J. Colling, P.J. Dornan, N. Konstantinidis, L. Moneta, A. Moutoussi, J. Nash, G. San Martin, J.K. Sedgbeer, A.M. Stacey

Department of Physics, Imperial College, London SW7 2BZ, United Kingdom[10]

G. Dissertori, P. Girtler, E. Kneringer, D. Kuhn, G. Rudolph

Institut für Experimentalphysik, Universität Innsbruck, 6020 Innsbruck, Austria[18]

C.K. Bowdery, T.J. Brodbeck, P. Colrain, G. Crawford, A.J. Finch, F. Foster, G. Hughes, T. Sloan, E.P. Whelan, M.I. Williams

Department of Physics, University of Lancaster, Lancaster LA1 4YB, United Kingdom[10]

A. Galla, A.M. Greene, K. Kleinknecht, G. Quast, J. Raab, B. Renk, H.-G. Sander, R. Wanke, C. Zeitnitz

Institut für Physik, Universität Mainz, 55099 Mainz, Fed. Rep. of Germany[16]

J.J. Aubert, A.M. Bencheikh, C. Benchouk, A. Bonissent,[21] G. Bujosa, D. Calvet, J. Carr, C. Diaconu, F. Etienne, M. Thulasidas, D. Nicod, P. Payre, D. Rousseau, M. Talby

Centre de Physique des Particules, Faculté des Sciences de Luminy, IN^{2}P^3-CNRS, 13288 Marseille, France

I. Abt, R. Assmann, C. Bauer, W. Blum, D. Brown,[24] H. Dietl, F. Dydak,[21] G. Ganis, C. Gotzhein, K. Jakobs, H. Kroha, G. Lütjens, G. Lutz, W. Männer, H.-G. Moser, R. Richter, A. Rosado-Schlosser, S. Schael, R. Settles, H. Seywerd, U. Stierlin,[2] R. St. Denis, G. Wolf

Max-Planck-Institut für Physik, Werner-Heisenberg-Institut, 80805 München, Fed. Rep. of Germany[16]

R. Alemany, J. Boucrot, O. Callot, A. Cordier, F. Courault, M. Davier, L. Duflot, J.-F. Grivaz, Ph. Heusse, M. Jacquet, D.W. Kim,[19] F. Le Diberder, J. Lefrançois, A.-M. Lutz, G. Musolino, I. Nikolic, H.J. Park, I.C. Park, M.-H. Schune, S. Simion, J.-J. Veillet, I. Videau

Laboratoire de l'Accélérateur Linéaire, Université de Paris-Sud, IN^2P^3-CNRS, 91405 Orsay Cedex, France

D. Abbaneo, P. Azzurri, G. Bagliesi, G. Batignani, S. Bettarini, C. Bozzi, G. Calderini, M. Carpinelli, M.A. Ciocci, V. Ciulli, R. Dell'Orso, R. Fantechi, I. Ferrante, L. Foà,[1] F. Forti, A. Giassi, M.A. Giorgi, A. Gregorio, F. Ligabue, A. Lusiani, P.S. Marrocchesi, A. Messineo, G. Rizzo, G. Sanguinetti, A. Sciabà, P. Spagnolo, J. Steinberger, R. Tenchini, G. Tonelli,[26] G. Triggiani, C. Vannini, P.G. Verdini, J. Walsh

Dipartimento di Fisica dell'Università, INFN Sezione di Pisa, e Scuola Normale Superiore, 56010 Pisa, Italy

A.P. Betteridge, G.A. Blair, L.M. Bryant, F. Cerutti, Y. Gao, M.G. Green, D.L. Johnson, T. Medcalf, Ll.M. Mir, P. Perrodo, J.A. Strong

Department of Physics, Royal Holloway & Bedford New College, University of London, Surrey TW20 OEX, United Kingdom[10]

V. Bertin, D.R. Botterill, R.W. Clifft, T.R. Edgecock, S. Haywood, M. Edwards, P. Maley, P.R. Norton, J.C. Thompson

Particle Physics Dept., Rutherford Appleton Laboratory, Chilton, Didcot, Oxon OX11 OQX, United Kingdom[10]

B. Bloch-Devaux, P. Colas, H. Duarte, S. Emery, W. Kozanecki, E. Lançon, M.C. Lemaire, E. Locci, B. Marx, P. Perez, J. Rander, J.-F. Renardy, A. Rosowsky, A. Roussarie, J.-P. Schuller, J. Schwindling, D. Si Mohand, A. Trabelsi, B. Vallage

CEA, DAPNIA/Service de Physique des Particules, CE-Saclay, 91191 Gif-sur-Yvette Cedex, France[17]

R.P. Johnson, H.Y. Kim, A.M. Litke, M.A. McNeil, G. Taylor

Institute for Particle Physics, University of California at Santa Cruz, Santa Cruz, CA 95064, USA[22]

A. Beddall, C.N. Booth, R. Boswell, S. Cartwright, F. Combley, I. Dawson, A. Koksal, M. Letho, W.M. Newton, C. Rankin, L.F. Thompson

Department of Physics, University of Sheffield, Sheffield S3 7RH, United Kingdom[10]

A. Böhrer, S. Brandt, G. Cowan, E. Feigl, C. Grupen, G. Lutters, J. Minguet-Rodriguez, F. Rivera,[25] P. Saraiva, L. Smolik, F. Stephan, P. van Gemmeren

Fachbereich Physik, Universität Siegen, 57068 Siegen, Fed. Rep. of Germany[16]

M. Apollonio, L. Bosisio, R. Della Marina, G. Giannini, B. Gobbo, F. Ragusa[20]

Dipartimento di Fisica, Università di Trieste e INFN Sezione di Trieste, 34127 Trieste, Italy

J. Rothberg, S. Wasserbaech

Experimental Elementary Particle Physics, University of Washington, WA 98195 Seattle, U.S.A.

S.R. Armstrong, L. Bellantoni,[30] P. Elmer, Z. Feng, D.P.S. Ferguson, Y.S. Gao, S. González, J. Grahl, J.L. Harton,[28] O.J. Hayes, H. Hu, P.A. McNamara III, J.M. Nachtman, W. Orejudos, Y.B. Pan, Y. Saadi, M. Schmitt, I.J. Scott, V. Sharma,[29] J.D. Turk, A.M. Walsh, Sau Lan Wu, X. Wu, J.M. Yamartino, M. Zheng, G. Zobernig

Department of Physics, University of Wisconsin, Madison, WI 53706, USA[11]

---

[1] Now at CERN, 1211 Geneva 23, Switzerland.
[2] Deceased.
[3] Now at Dipartimento di Fisica, Università di Lecce, 73100 Lecce, Italy.
[4] Also Istituto di Fisica Generale, Università di Torino, Torino, Italy.
[5] Also Istituto di Cosmo-Geofisica del C.N.R., Torino, Italy.
[6] Now at TSM Business School, Enschede, The Netherlands.
[7] Supported by CICYT, Spain.
[8] Supported by the National Science Foundation of China.
[9] Supported by the Danish Natural Science Research Council.
[10] Supported by the UK Particle Physics and Astronomy Research Council.
[11] Supported by the US Department of Energy, contract DE-AC02-76ER00881.
[12] On leave from Universitat Autonoma de Barcelona, Barcelona, Spain.
[13] Supported by the US Department of Energy, contract DE-FG05-92ER40742.
[14] Supported by the US Department of Energy, contract DE-FC05-85ER250000.
[15] Permanent address: Universitat de Barcelona, 08208 Barcelona, Spain.
[16] Supported by the Bundesministerium für Forschung und Technologie, Fed. Rep. of Germany.
[17] Supported by the Direction des Sciences de la Matière, C.E.A.
[18] Supported by Fonds zur Förderung der wissenschaftlichen Forschung, Austria.
[19] Permanent address: Kangnung National University, Kangnung, Korea.
[20] Now at Dipartimento di Fisica, Università di Milano, Milano, Italy.
[21] Also at CERN, 1211 Geneva 23, Switzerland.
[22] Supported by the US Department of Energy, grant DE-FG03-92ER40689.
[23] Now at University of Athens, 157-71 Athens, Greece.
[24] Now at Lawrence Berkeley Laboratory, Berkeley, CA 94720, USA.
[25] Partially supported by Colciencias, Colombia.
[26] Also at Istituto di Matematica e Fisica, Università di Sassari, Sassari, Italy.
[27] Now at Schuster Laboratory, University of Manchester, Manchester M13 9PL, UK.
[28] Now at Colorado State University, Fort Collins, CO 80523, USA.
[29] Now at University of California at San Diego, La Jolla, CA 92093, USA.
[30] Now at Fermi National Accelerator Laboratory, Batavia, IL 60510, USA.
[31] Supported by the Commission of the European Communities, contract ERBCHBICT941234.

1 Introduction

The transformation of quarks and gluons to colourless hadrons in the non-perturbative region of QCD is not calculable, and must be simulated using hadronization models. The measurement of inclusive particle production cross sections provides useful information to test parton fragmentation models and improves the understanding of the hadronization process. Resonant states and their dynamics are more closely related to the original partons than lighter hadrons. Light vector mesons are copiously produced in hadronic events and thus well suited to a study of hadronization.

Though, after appropriate parameter tuning [1], the global event properties produced by hadronization models agree reasonably well with the data, the details of the spectra of identified particles are not well-constrained. The measurement of light vector mesons gives direct information about such parameters as the vector to pseudoscalar ratio in the fragmentation and the suppression factor for strange quark pair production in models such as JETSET [2].

Measurements of inclusive particle production have been made at centre-of-mass energies lower than at LEP (see References [3, 4] and references therein). The measurements had comparatively low statistics and differed among themselves because of systematic uncertainties. With the large number of hadronic events at LEP a more accurate analysis can be performed. The large data sample is particularly important for the understanding of the two-pion mass spectrum, which is found to be strongly influenced by Bose-Einstein correlations [5].

In this paper measurements of the inclusive momentum distributions are presented for the neutral vector mesons[1] ρ^0, ω, K^{*0}, and ϕ produced in hadronic Z decays. The ρ^0, K^{*0}, and ϕ have also been studied by other LEP collaborations [6, 7, 8]. Comparison with previous studies of other mesons allows an investigation of the relative production rates of vector and pseudoscalar particles and of the strangeness suppression in the fragmentation process.

The analyses are based on hadronic events recorded by the ALEPH detector at centre-of-mass energies around $\sqrt{s} = 91.2\,\mathrm{GeV}$ in the 1992 running period of LEP.

2 ALEPH Detector and Event Selection

The ALEPH detector has been described in detail elsewhere [9]. The present analyses use mainly the tracking components and the electromagnetic calorimeter. Charged particles are measured over the polar angle range $|\cos\theta| < 0.966$ by the cylindrical inner drift chamber and the large cylindrical time projection chamber (TPC), which measures up to 21 three dimensional space points per track. These chambers are immersed in a magnetic field of 1.5 T and together measure the momentum of charged particles with a resolution of $\delta p/p = 0.0008 \cdot p \oplus 0.005$ (p in GeV/c). For tracks with $|\cos\theta| < 0.85$, which are also measured by a vertex detector, the momentum resolution is improved to $\delta p/p = 0.0006 \cdot p \oplus 0.005$ (p in GeV/c). The TPC is surrounded by the electromagnetic calorimeter (ECAL),

[1] In the following, a specific isospin state implies the inclusion of the antiparticle as well.

which covers the angular range $|\cos\theta| < 0.98$ and has a thickness of 22 radiation lengths. With its fine segmentation in projective towers of approximately 0.9° by 0.9°, the angular resolution is $\sigma_{\theta,\phi} = 2.5/\sqrt{E} \oplus 0.25$ (E in GeV; $\sigma_{\theta,\phi}$ in mrad). This lead-proportional tube chamber has an energy resolution for electromagnetic showers of $\sigma_E/E = 0.18/\sqrt{E} + 0.009$ (E in GeV).

For the event selection, good tracks are defined as originating close to the interaction point (with transverse impact-parameter $|d_0| < 2\,\mathrm{cm}$ and longitudinal impact-parameter $|z_0| < 5\,\mathrm{cm}$), having at least 4 TPC hits, a polar angle in the range $20° < \theta < 160°$, and a transverse momentum $p_t > 200\,\mathrm{MeV}/c$. Hadronic Z decays are selected by requiring at least five good tracks. The total energy carried by all good tracks is required to exceed 15 GeV and the sphericity axis must be in the range $35° < \theta < 145°$. With these cuts, a sample of 519,924 events is selected from the 1992 running period, which corresponds to an integrated luminosity of $22\,\mathrm{pb}^{-1}$. The background to these events arises from tau decays and two-photon events and is estimated to be less than 0.3% [10].

2.1 Event and detector simulation

Samples of events generated with the JETSET 7.3 Monte Carlo, modified with DYMU3 [11] for electromagnetic radiative effects and improved bottom and charm decay tables, were passed through a full detector simulation and reconstruction program for model comparison and as a means of measuring the detector acceptance. The generator was tuned to describe the ALEPH data using the charged particle momentum inclusive distribution and event shape distributions [1].

The strangeness suppression and the ratio of vector to pseudoscalar mesons [V/(V+P)] were kept at their default values. The η' rate was adjusted to agree with the previous ALEPH measurement [12]: 80% of the η' were rejected. The Bose-Einstein effect was not simulated at this point. The generated events were subjected to the same selection and analysis chain as the data. After the event selection a sample of 1,604,738 events remains.

A sample of 113,126 HERWIG 5.6 [13] events was passed through the same detector simulation and reconstruction programs as a check on the model dependence of the investigations. The model parameters were tuned using ALEPH data in the same manner as mentioned above [1].

For comparison with the measured inclusive meson spectra, 1,000,000 events with JETSET 7.4 were generated, where production of tensor mesons was enabled and improved decay tables added. The generator was tuned to describe event shape distributions and multiplicities of identified particles as measured at the e^+e^- colliders PEP, PETRA, and LEP.

To parameterize the effect of Bose-Einstein correlations in the uncorrected data, sets of 1,000,000 events were generated without detector simulation or various values of the chaoticity parameter λ, which gives the strength of the Bose-Einstein effect, and the inverse region size $1/\sigma$. The Gaussian parameterization of Bose-Einstein correlations for the nine light pseudoscalar mesons was chosen. The coherence time parameter χ was set to $0.1\,\mathrm{GeV}/c^2$. This parameter gives the minimum width of resonances whose daughters contribute to the Bose-Einstein enhancement. Typical values for the chaoticity parameter

λ, giving the incoherence of the source, and the inverse region size $1/\sigma$ were chosen to be 2.1 and 0.35 GeV/$\hbar c$. The detector effects are taken into account, correcting the invariant mass spectrum generated with Bose-Einstein with the ratio of the two-pion mass spectra of JETSET 7.3 with detector simulation and with no detector effects.

2.2 Particle identification

Vector mesons decay strongly with their daughters originating from the primary interaction point. To reject decay products from neutral weakly decaying particles and photon conversions, reducing the combinatorial background, pion and kaon candidates are required to be reconstructed as good tracks (as discussed above). However, tighter cuts on the distance to the collision point ($|d_0| < 0.3$ cm and $|z_0| < 3$ cm for ρ^0 and ω) are applied. The requirement on d_0 and z_0 can be loosened when one or more of the daughters are kaons, as the combinatorics are then lower: the corresponding values are 0.5 cm and 5 cm for K^{*0}, 1 cm and 5 cm for ϕ.

Particle identification is important in order to reduce the combinatorial background, particularly for analyses using charged kaons. For charged particles this is done by simultaneous measurement of momentum and ionization energy loss. A particle's energy loss is sampled in the TPC by up to 338 wires. The deviation from an assumed hypothesis is expressed as $\chi(\mathrm{d}E/\mathrm{d}x)$:

$$\chi(\mathrm{d}E/\mathrm{d}x) = \frac{\left(\frac{\mathrm{d}E}{\mathrm{d}x}\right)_{\mathrm{measured}} - \left(\frac{\mathrm{d}E}{\mathrm{d}x}\right)_{\mathrm{expected}}}{\sigma_{\mathrm{d}E/\mathrm{d}x}}.$$

Here $\sigma_{\mathrm{d}E/\mathrm{d}x}$ is the expected $\mathrm{d}E/\mathrm{d}x$ resolution normalized with a sample of minimum ionizing pions [9].

The separation of the $\mathrm{d}E/\mathrm{d}x$ bands is a function of momentum. The backgrounds in the various analyses differ, so the cut on $\chi(\mathrm{d}E/\mathrm{d}x)$ depends on which signal is being studied.

Neutral pions are reconstructed from pairs of neutral clusters in the ECAL. The γ energy is estimated from the energy collected in the four central towers of a cluster, correcting to the full energy from the parameterization of the shower shape for a single photon in the calorimeter. Whilst the energy resolution is degraded to $\sigma_E/E \approx 0.25/\sqrt{E}$ (E in GeV) by using this technique, hadronic background and clustering effects are reduced. π^0 candidates are accepted if the invariant mass of the photon pair is within 1.7σ of the expected mass, where σ is typically 25 MeV/c^2 (see Figure 1). The π^0 energy resolution is improved to $\sigma_E/E \approx 0.06$ by constraining the mass of the π^0 candidates to 135 MeV/c^2.

3 Signal extraction and fitting procedures

The cross sections of the vector mesons are extracted from the invariant mass distributions of their daughters. The data are analyzed in eight intervals of $x_p = p(\mathrm{hadron})/p(\mathrm{beam})$. To extract the cross section for a given meson, the distribution is fitted as the sum of a background and a signal function.

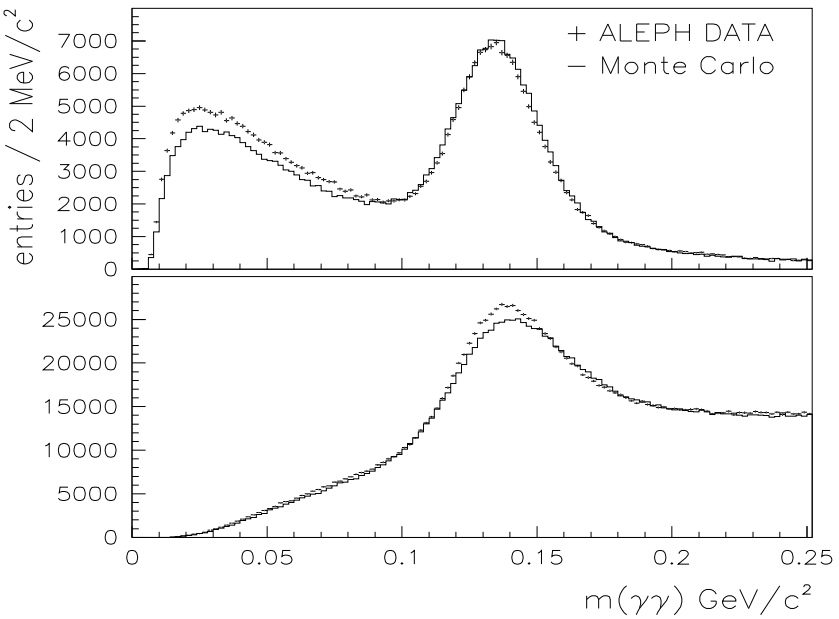

Figure 1: *Invariant mass of pairs of photons. The upper plot is for photon pairs taken from a single ECAL cluster within which two subclusters are resolved; this occurs for high momentum π^0's where the opening angle between the two photons is small. The lower plot is for cases where each photon is taken from an isolated ECAL cluster with no resolvable subclusters.*

The background can in general be represented by a smooth function. The specific choice is somewhat arbitrary and depends on the shape and amount of the combinatorial background. Some fits need the inclusion of reflections, e.g., in the K^{*0} analysis: charged pions from the $\pi^+\pi^-\pi^0$ decay of the ω will give a structure in the $m(\mathrm{K}^{\pm}\pi^{\mp})$ spectrum and must be taken into account as a separate contribution.

The signal is a convolution of a Breit-Wigner function, which describes the shape of the meson produced, and a resolution function, which accounts for the uncertainty in the momentum measurement in the detector. The Breit-Wigner function [14] used is

$$BW(m) = \frac{m \cdot m_0 \cdot \Gamma(m)}{(m^2 - m_0^2)^2 + m_0^2 \cdot \Gamma^2(m)},$$

with

$$\Gamma(m) = \Gamma_0 \cdot \left(\frac{q}{q_0}\right)^{2l+1} \frac{m_0}{m},$$

where $l = 1$ for vector mesons (referred to as p-wave); q is the momentum of the decay products in the rest frame of the parent, and q_0 is the momentum when $m = m_0$.

The way the resolution is taken into account depends on the natural width of the meson relative to the detector resolution. Thus the treatment differs for the four mesons

under study. For the K^{*0}, the uncertainty from the resolution can be neglected. For the ϕ, a convolution is made, which depends on momentum. For the ω, the energy resolution of the ECAL dominates the shape of the signal and a sum of Gaussians is taken.

For the ρ^0, which has a large width ($151.5 \pm 1.2\,\mathrm{MeV}/c^2$), the detector resolution is not important. However, Bose-Einstein correlations may distort the ρ^0 line shape, through interactions between the ρ^0 decay pions and other pions. Therefore, a different strategy was used: using JETSET modified to include the Breit-Wigner function described above for the ρ^0 and the K^{*0}, both signal and background shape were taken from the Monte Carlo. A slightly different parameterization of the width is taken for the ρ^0 [15]:

$$\Gamma(m) = \Gamma_0 \cdot \frac{2 \cdot (\frac{m^2 - 4 \cdot m_\pi^2}{m_0^2 - 4 \cdot m_\pi^2})^{\frac{3}{2}}}{1 + \frac{m^2 - 4 \cdot m_\pi^2}{m_0^2 - 4 \cdot m_\pi^2}}.$$

The number of signal events for the wide resonances (ρ^0, K^{*0}) is defined as the number in a mass range $\pm 2.5\Gamma_0$ around their nominal masses.

3.1 Extraction of the $\rho^0(770)$ signal

To extract the ρ^0 signal, the two-particle mass spectrum of like-sign pions $m(\pi^\pm, \pi^\pm)$ is subtracted from the spectrum of the unlike-sign pions $m(\pi^+, \pi^-)$ reducing systematics common to both two-pion spectra. All tracks originating from the beam collision point are considered as pions, provided that their ionization energy loss measurement, if available, is compatible with the pion hypothesis, $|\chi(\mathrm{d}E/\mathrm{d}x)| < 3$. Possible ρ^0 candidates are formed from pion pairs in the same hemisphere as defined by the thrust axis.

A considerable discrepancy is seen between the like-sign subtracted mass spectra obtained from the data and the Monte Carlo prediction (JETSET 7.3, tuned to ALEPH data). The ρ^0 resonance in the data seems to be shifted towards lower masses. In the mass region below the resonance, the data clearly exceed the Monte Carlo, whilst at masses just above threshold, Monte Carlo exceeds the data (Figure 2). The effect seen is a function of the scaled momentum $x_p = p_\rho / p_{\mathrm{beam}}$ of the $\pi^+\pi^-$ pair considered as a ρ^0 candidate, the discrepancy increasing towards smaller momenta.

In Reference [16] several effects that can affect the ρ^0 line shape are discussed. The possibilities considered are Bose-Einstein correlations, ρ^0-ω interference and interference with coherent $\pi^+\pi^-$ backgrounds. Further considerations are discussed in [17].

After enabling Bose-Einstein correlations, JETSET describes the subtracted spectrum fairly well, except for a small correction, which will be described in a following paragraph on the fitting procedure. Introduced as a final state interaction acting on identical pseudoscalar mesons, the simulation of the Bose-Einstein effect changes both the $m(\pi^\pm, \pi^\pm)$ and the $m(\pi^+, \pi^-)$ spectrum. The ρ^0 line shape is changed as well. However, a fair description of the data is only obtained with the chaoticity parameter λ, which is a measure of the strength (ranging from $\lambda = 0$ to 1) of the Bose-Einstein effect, twice as large as the expected maximum.

It has already been pointed out by the OPAL collaboration [18] that inclusion of Bose-Einstein correlations in JETSET improves the description of the invariant mass spectrum

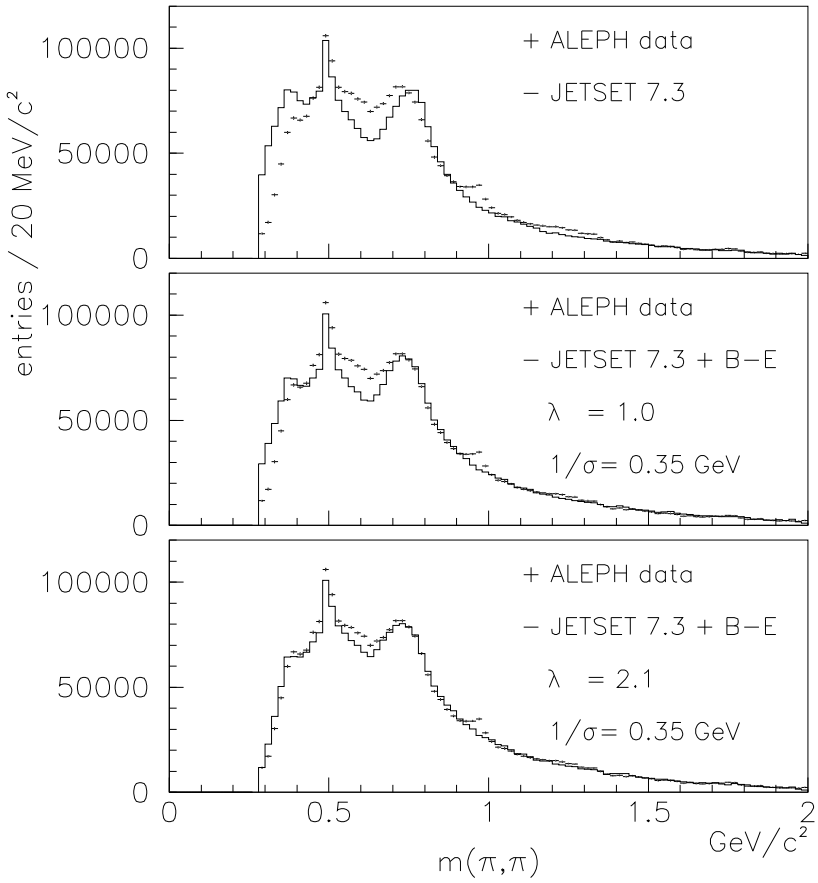

Figure 2: *The subtracted two-pion mass spectra (unlike minus like-sign) for data (crosses) and tuned* JETSET *(solid curve) with and without Bose-Einstein correlations are shown, including detector simulation.*

of pions. Their value $\lambda = 2.5$ is compatible with our value in view of the different η' rate and choice of the coherence time parameter χ (see Section 2.1). A mass shift in the ρ^0 is observed by the DELPHI collaboration, even when the ρ^0 line shape is parameterized with $\lambda = 1$ in JETSET [6, 7, 19].

The high λ-parameter ($\lambda \approx 2.1$) in the JETSET model needed for this analysis is in agreement with those observations, and supports the observation by the OPAL experiment. The uncorrected direct measurements of the chaoticity parameter λ from the enhancement in the ratio $Q(\pi^{\pm},\pi^{\pm})/Q(\pi^{\pm},\pi^{\mp})$ yield values less than 1. It would seem, however, that when they are corrected for the number of like-sign pion pairs which can participate in the Bose-Einstein effect, as predicted by Monte Carlo, that values in excess of 1 are obtained (see e.g., [20] or [17] for a short review). The explanation for those measurements, as well as the large value required for this work may be an underestimation of the number of like-sign pion pairs affected by Bose-Einstein correlations or other complications such as final state interactions (e.g., strong interaction).

Because of the correlated change of the ρ^0 line shape (seen in the data as a shift of

the peak position of the ρ^0) and the background as suggested by JETSET, the ρ^0 rate is extracted as described in the following paragraphs.

The background shape (B) and the ρ^0 line shape (R) are taken from JETSET, modified for ρ^0 and K^{*0} with a p-wave Breit-Wigner distribution from the production threshold to 2 GeV/c^2. Using samples with different values of the chaoticity parameter λ and the inverse region size $1/\sigma$ (the coherence time parameter χ was chosen to be 0.1 GeV/c^2, so that the K^{*0} is not affected), a χ^2 fit is made to the distribution $\Delta D(m)$, defined as the difference of the unlike and like-sign invariant mass spectra of the data. The function used to fit the subtracted two-pion mass spectrum is a sum of contributions from the ρ^0 signal, combinatorial background, and other resonances,

$$\Delta D(m) = n_\rho \cdot R(m;\lambda,1/\sigma) + \Delta B(m;\lambda,1/\sigma) + \text{other resonances}(\omega, f_0, f_2, K^{*0}),$$

where the normalization n_ρ, chaoticity parameter λ, and the inverse region size $1/\sigma$ are the free parameters. The like-sign subtracted combinatorial background, ΔB, is

$$\Delta B(m;\lambda,1/\sigma) = B^{+-}(m;\lambda,1/\sigma) - a_1 \cdot (1 + a_2 \cdot Q) \cdot B^{\pm\pm}(m;\lambda,1/\sigma)$$

where a_1 and a_2 are free parameters to allow for a free normalization and a linear correction in $Q = \sqrt{(p_i + p_j)^2 - 4m_\pi^2}$ in the model.

Figure 3 shows the result of the fit[2] to the difference spectrum for all momenta x_p. Resonances and reflections close in mass (ω, f_0, f_2, K^{*0}) are included in the fit with their normalizations as free parameters. The production rate for f_0 is about 10% of the ρ^0 rate. The fit leads to a value of the ω rate consistent, although with larger uncertainties, with that obtained using the three pion decay as discussed in the following section. The fit range was chosen to be 380 to 1800 MeV/c^2, but excluding the K^0_S range, 480 to 520 MeV/c^2.

3.2 Extraction of the $\omega(782)$ signal

The ω meson is measured in its three pion decay mode. Only $x_p > 0.05$ is considered, because the signal to background ratio is too small for low momenta. The natural width of the ω is $\Gamma_0 = 8.43 \pm 0.10$ MeV/c^2. The reconstructed width (FWHM ≈ 35 MeV/c^2) is dominated by the π^0 resolution. The π^0 reconstruction is described in Section 2.2. For this analysis only photon candidates with energy greater than 0.6 GeV are selected. Neutral pion candidates are required to have an energy less than 16 GeV. The poor purity of π^0's at low energy is improved by reducing the combinatorics with a 'ranking' method, removing candidates which share photons, and keeping only those having a smaller opening angle. The charged pions are selected as for the ρ^0, but with no cuts on $\mathrm{d}E/\mathrm{d}x$.

The ω rate is extracted from the $m(\pi^+,\pi^-,\pi^0)$ spectra using a third order polynomial for the background, and a signal function empirically parameterized as the sum of three Gaussians. The relative widths and normalizations of the three Gaussians are determined

[2]Fitted values for the chaoticity parameter and the inverse region size are $\lambda = 2.1 \pm 0.1 \pm 0.1$ and $1/\sigma = 0.35 \pm 0.01 \pm 0.03$ GeV/$\hbar c$. The first error is statistical, the second gives the variation of the fitted values between different x_p bins.

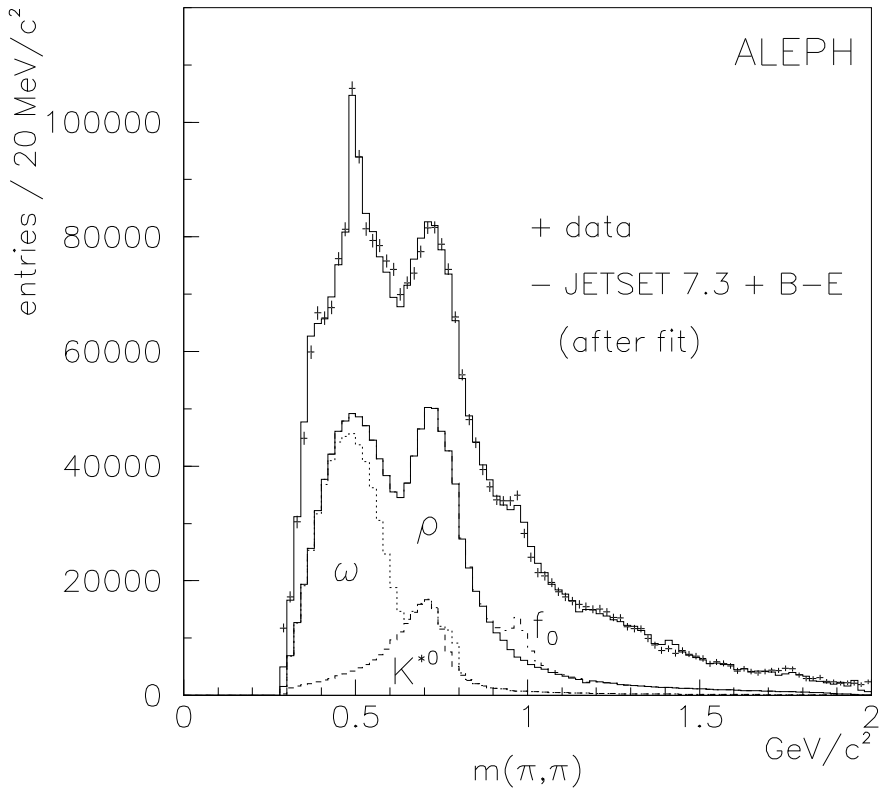

Figure 3: *Comparison of like-sign subtracted mass spectra for data (crosses) and tuned* JETSET *(solid curve) including detector simulation and Bose-Einstein correlations after fit (see Section 3.1) for all momenta x_p including detector simulation. The contributions from* K^{*0}, ω, ρ^0, *and* f_0 *are added cumulatively. The contributions from the combinatorial background,* f_2, *and* K^0_S *are not shown separately.*

from the Monte Carlo and fixed before the fit. The normalization and mass of the signal are free in the fit, whilst the width is fixed to the Monte Carlo signal width determined in each momentum region. Another function is introduced at lower mass to take into account the η meson. The fit is improved by subtracting the like-sign mass spectrum $m(\pi^\pm,\pi^\pm,\pi^0)$ from the unlike one (Figure 4).

3.3 Extraction of the $\mathrm{K}^{*0}(892)$ signal

The K^{*0} meson is measured using its charged decay mode ($\mathrm{K}^{*0} \to \mathrm{K}^\pm\pi^\mp$). Since most charged particles in hadronic Z decays are pions, an efficient and clean particle identification of the $\mathrm{K}^\pm$ is crucial for the extraction of the K^{*0} signal. In contrast to the ϕ, where the narrowness of the resonance allows an extraction even without particle identification, a good ionization measurement in the TPC is important. The large width of the K^{*0} ($50.5 \pm 0.6\,\mathrm{MeV}/c^2$) and the proximity of the ρ^0 reflection gives rise to a large background from $\pi^+\pi^-$ pairs. This is reduced by a cut on the decay angle: the

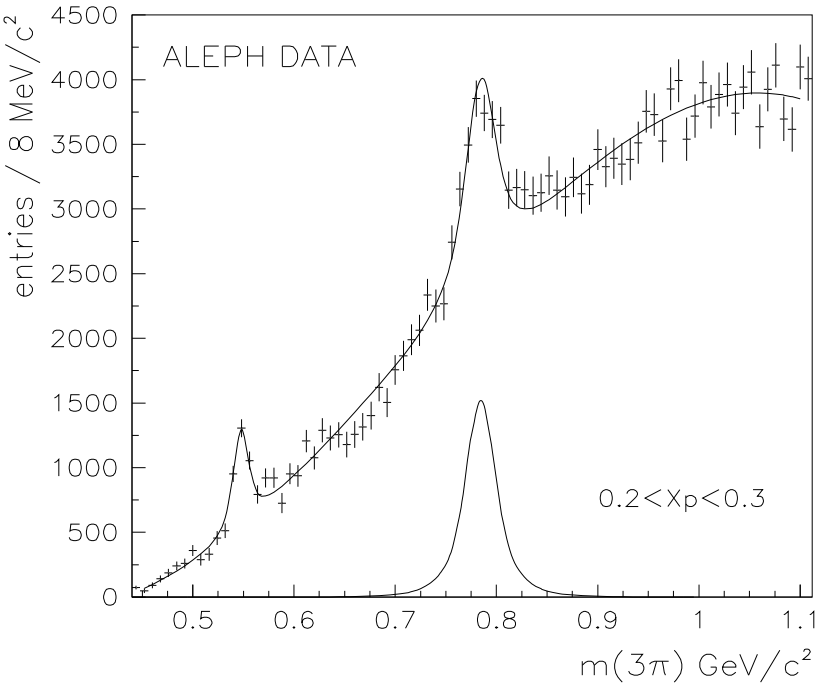

Figure 4: *Invariant mass spectrum $m(\pi^+\pi^-\pi^0)$ (like-sign subtracted). The data (crosses) are well described by the fit (solid curve). The signal extracted from the fit is shown below the spectra. A function is introduced to account for the η, clearly visible around* $550\,\mathrm{MeV}/c^2$.

K^{*0} candidate is retained if the angle θ^* between the kaon and the K^{*0} direction in the K^{*0} rest frame satisfies $|\cos\theta^*| < 0.8$. This cut and other momentum cuts are sensitive to the $\cos\theta^*$ distribution in the Monte Carlo, however, in the fragmentation process this distribution is expected to be isotropic so this is not a serious problem. The like-sign mass spectrum was subtracted from the unlike-sign one, because the combinatorial background is easier to parameterize.

All good tracks coming from the interaction point ($|d_0| < 0.5\,\mathrm{cm}$, $|z_0| < 5\,\mathrm{cm}$) are considered kaon or pion candidates. The allowed deviation from a particle hypothesis expressed as $\chi(\mathrm{d}E/\mathrm{d}x)$ must be carefully chosen. Pions are accepted if $|\chi(\mathrm{d}E/\mathrm{d}x)| < 3$, independent of momentum and x_p. The requirements for kaon candidates depend on the x_p range. For $x_p < 0.1$, $|\chi(\mathrm{d}E/\mathrm{d}x)| < 1.5$ is required, whilst for $x_p > 0.1$ tracks with $|\chi(\mathrm{d}E/\mathrm{d}x)| < 2$ are selected. However, for the range $0.025 < x_p < 0.05$, kaon candidates with $0.8\,\mathrm{GeV}/c < p(\mathrm{K}^\pm) < 1.4\,\mathrm{GeV}/c$ are excluded, because here the ionization of pions and kaons is almost the same. The kaon candidates so obtained for this x_p interval are then subject to tighter cuts, dependent on the kaon momentum. For tracks with $p(\mathrm{K}^\pm) < 0.8\,\mathrm{GeV}/c$, one requires $-1 < \chi(\mathrm{d}E/\mathrm{d}x) < 2$; and for $p(\mathrm{K}^\pm) > 1.4\,\mathrm{GeV}/c$, one requires $-2 < \chi(\mathrm{d}E/\mathrm{d}x) < 0$, respectively. Tracks which satisfy both hypotheses (kaon and pion) are considered pions *and* kaons and enter the mass distribution more than once.

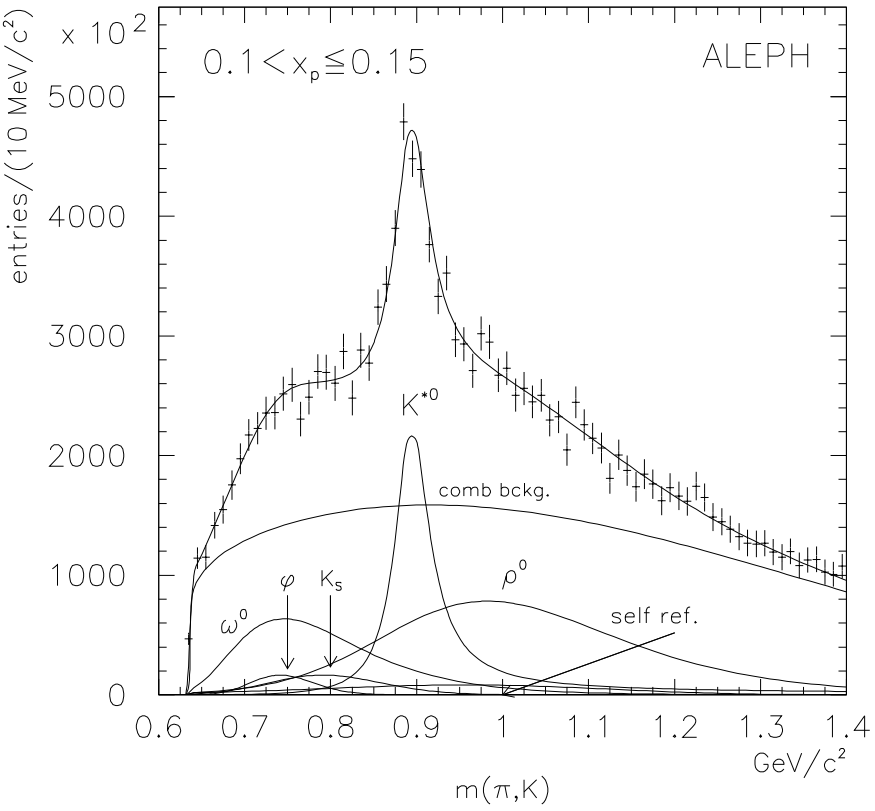

Figure 5: *Invariant mass spectrum* $m(\mathrm{K}^{\pm}\pi^{\mp})$ *(like-sign subtracted). The data (crosses) are well described by the fit (solid curve). The contributions from reflections and combinatorial background are shown as well.*

To extract the K^{*0} rate, a fit is performed using a p-wave Breit-Wigner function with parameters for mass and width from Reference [4], the self-reflection, other resonances and combinatorial background (Figure 5). The function

$$f(m_{\mathrm{K}^{\pm}\pi^{\mp}}) = a_1\,(m_{\mathrm{K}^{\pm}\pi^{\mp}} - m_{\mathrm{thr}})^{a_2} \cdot \exp\left[-a_3(m_{\mathrm{K}^{\pm}\pi^{\mp}} - m_{\mathrm{thr}}) - a_4(m_{\mathrm{K}^{\pm}\pi^{\mp}} - m_{\mathrm{thr}})^2\right],$$

with $m_{\mathrm{thr}} = m_{\mathrm{K}^{\pm}} + m_{\pi^{\mp}}$ gives a good background description; the a_i are free parameters of the fit. Resonances close to the K^{*0} signal (ρ^0, ω, $\mathrm{K}^0_{\mathrm{S}}$, and ϕ) as well as the self-reflection are included in the fit. The shapes are parameterized by an analytic function, whilst the rates for $\mathrm{K}^0_{\mathrm{S}}$, ρ^0, and ϕ are taken from measurements and fixed. The ω is fixed by the ratio ω/ρ^0 as given by JETSET 7.3. For the shape of the ρ^0, the distortions due to Bose-Einstein correlations are taken into account.

3.4 Extraction of the $\phi(1020)$ signal

The decay mode of $\phi \to \mathrm{K^+K^-}$ is the dominant decay channel ($BR = 49.1 \pm 0.9\%$). Two methods are used for selecting the kaons in order to find the ϕ: one using particle identification with $\mathrm{d}E/\mathrm{d}x$ and the other assuming all charged particles to be kaons.

The good separation of pions and kaons in the $1/\beta^2$ region of the $\mathrm{d}E/\mathrm{d}x$ plot allows for a selection with high efficiency and purity by requiring $|\chi(\mathrm{d}E/\mathrm{d}x)| < 5$ for low momentum kaons ($p_\mathrm{K} < 0.6\,\mathrm{GeV}/c$). For $p_\mathrm{K} > 0.6\,\mathrm{GeV}/c$, the cut $|\chi(\mathrm{d}E/\mathrm{d}x)| < 3$ is used.

The narrow width of the ϕ ($4.43 \pm 0.06\,\mathrm{MeV}/c^2$) ensures that its reconstruction is still possible without kaon identification, especially for higher momenta, where the combinatorial background is not too large. This method avoids any uncertainty on the ionization loss measurement that may arise from overlapping tracks.

Since the results of the two methods are compatible within the errors, no $\mathrm{d}E/\mathrm{d}x$ measurement for $x_p > 0.1$ is used, but particle identification with $\mathrm{d}E/\mathrm{d}x$ is included for lower ϕ momenta.

The invariant mass distribution $m(\mathrm{K^+,K^-})$ is the sum of the signal plus background. The signal is taken as a convolution of the original ϕ signal (a p-wave Breit-Wigner function), and a resolution function $r(m,m')$. The resolution function is necessary to allow for the limited resolution of the reconstructed mass, due to the uncertainties in the reconstructed kaon four-momenta. In fact, the mass uncertainty is comparable to the width of the ϕ resonance, so the shape of the signal is significantly changed. Monte Carlo studies have revealed that a simple Breit-Wigner, with width Γ_res, is a good representation for $r(m,m')$. The resolution function then becomes

$$r(m,m') = \frac{1}{\pi}\frac{\Gamma_\mathrm{res}}{(m-m')^2 + (\Gamma_\mathrm{res}/2)^2} \ .$$

The resolution parameter Γ_res was determined from Monte Carlo (Figure 6), because the signal to background ratio for the ϕ does not allow the determination of the resolution from the data. The value of Γ_res varies from $1\,\mathrm{MeV}/c^2$ for small x_p to $4\,\mathrm{MeV}/c^2$ for high x_p.

For the background, studies on the Monte Carlo suggested the following choice of background function:

$$f(m_{\mathrm{K^\pm K^\mp}}) = a_1(m_\mathrm{diff})^{a_2} \cdot \exp(a_3 m_\mathrm{diff} + a_4 m_\mathrm{diff}^2 + a_5 m_\mathrm{diff}^3 + a_6 m_\mathrm{diff}^4),$$

where the a_i are free parameters and $m_\mathrm{diff} = m_{\mathrm{K^\pm K^\mp}} - 2m_{\mathrm{K^\pm}}$. In the fits (see Figure 7 as an example), the ϕ mass and width are fixed to the Particle Data Group values [4].

4 Discussion of Results

4.1 Inclusive momentum spectra

The invariant mass spectra for eight x_p intervals from 0.005 to 1 are fitted for the vector mesons with the procedures discussed above. Fitted mass spectra are shown as examples in Figures 3, 4, 5, and 7.

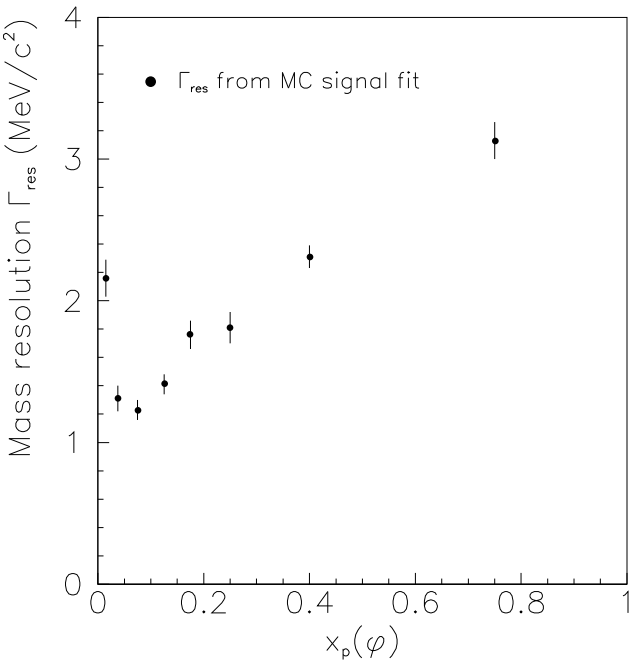

Figure 6: *The mass resolution* $\Gamma_{\rm res}$ *for* ϕ *as determined from Monte Carlo. Kaons from* ϕ *decay are passed through the detector simulation and fitted with the signal function described in the text. The resolution* $\Gamma_{\rm res}$ *is a free parameter. The* ϕ *mass and width were fixed to the Particle Data Group values [4].*

The acceptance-corrected cross sections are given in Tables 1, 3, 5, and 7, in which the first error quoted is statistical and the second systematic. JETSET 7.3 tuned to ALEPH data [1] including full detector simulation has been used to extract the reconstruction efficiencies. In Figure 8 the momentum spectra are shown and compared to model predictions from tuned JETSET 7.3 and HERWIG 5.6. In addition, the spectra obtained with JETSET 7.4 tuned to ALEPH data are displayed, in which the production of tensor mesons was enabled and improved decay tables added. The error bars in Figure 8 show the quadratic sum of statistical and systematic errors.

The meson production rates are extracted by adding the rates from all measured x_p bins and extrapolating to $x_p = 0$. The range $0.005 \leq x_p \leq 1$ comprises more than 99% of the total rate for ρ^0, K^{*0}, and ϕ. For the ω, where the measurement starts at $x_p = 0.05$, JETSET 7.4 is used for extrapolation (Section 4.2.2). The systematic errors over the full x_p range for each source (see Tables 2, 4, 6, and 8; *all* x_p) are obtained by assuming the individual errors of the x_p bins are correlated. For the ϕ where two different selections have been used (with and without $\mathrm{d}E/\mathrm{d}x$), the systematic errors in the x_p ranges 0.005-0.1 and 0.1-1.0 are assumed 100% positively correlated.

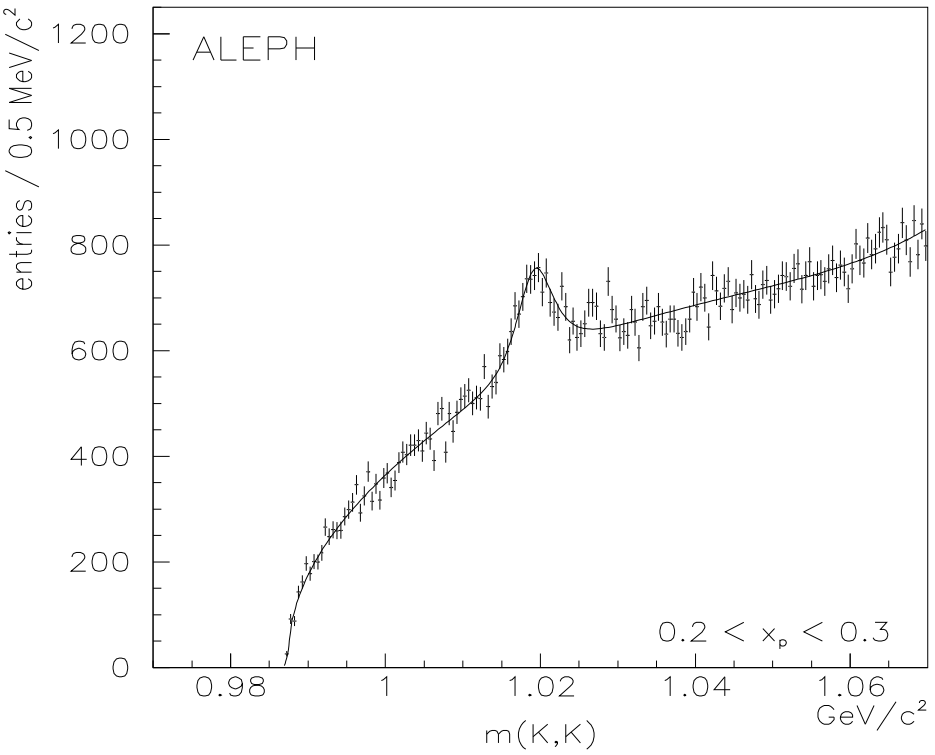

Figure 7: *Mass spectrum* $m(\mathrm{K}^+,\mathrm{K}^-)$. *The data (crosses) are fitted with the function described in Section 3.4 (solid curve).*

4.2 Systematic Errors

4.2.1 Systematic errors for the $\rho^0(770)$

The results of the systematics studies are listed in Table 2. The effect of nearby resonances is studied by changing the K^{*0} cross section and the ω cross section by 15%. The f_0 mass was varied by $10\,\mathrm{MeV}/c^2$ and its width by a factor of 2. The error given in the table is obtained by adding the variations in quadrature.

The extraction of the cross section was repeated using a cut of $|\chi(\mathrm{d}E/\mathrm{d}x)| < 2$ and omitting this cut completely. The influence from the uncertainty on the ρ^0 mass and width (varied by $2\,\mathrm{MeV}/c^2$ and $10\,\mathrm{MeV}/c^2$, respectively) was found to be small. The fit range was varied from 380 to $520\,\mathrm{MeV}/c^2$ for the lower bound, and from 1600 to $2000\,\mathrm{MeV}/c^2$ for the upper bound. Track and event selection cuts were varied to study the influence on the measured ρ^0 multiplicity. Furthermore, the influence of the exact Monte Carlo tuning was investigated by changing model parameters such as Λ_{QCD} and

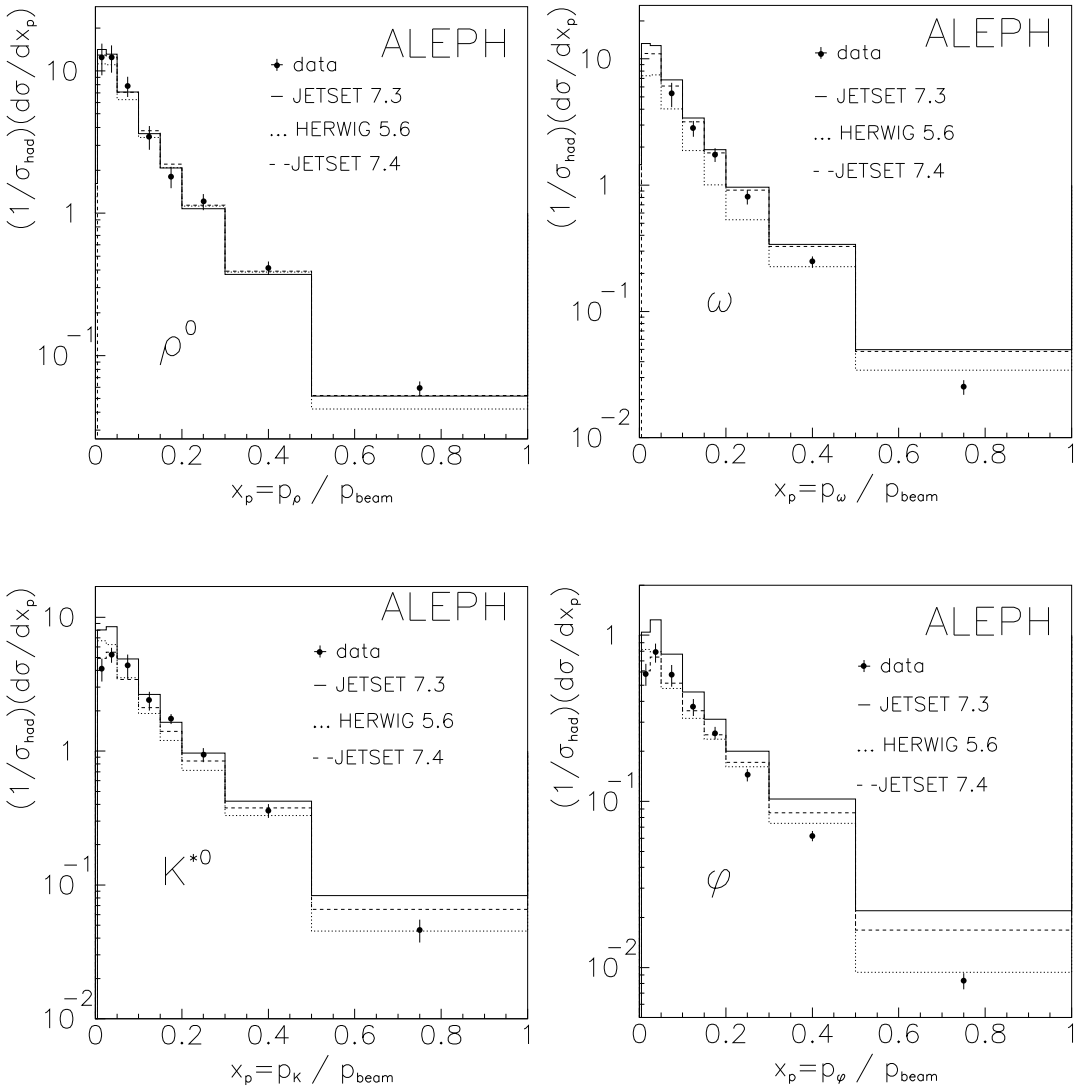

Figure 8: *Differential cross section for* ρ^0, ω, K^{*0}, *and* ϕ *in comparison with Monte Carlo predictions. The errors shown are the quadratic sum of statistical and systematic contributions.* JETSET 7.4, *where production of tensor mesons was enabled and improved decay tables added, was tuned to describe event shape distributions and multiplicities of identified particles as measured at the* e^+e^- *colliders PEP, PETRA, and LEP.*

σ_t, the transverse momentum of primary hadrons. The effect was found to be small and was neglected.

The chaoticity parameter, λ, and inverse region size $1/\sigma$ are free parameters in the fit to the ρ^0 signal, and contribute to the statistical error. No other variations in the description of the Bose-Einstein effect were made, and no systematic error, arising from possible uncertainties in the Bose-Einstein effect, was included.

4.2.2 Systematic errors for the $\omega(782)$

The results from the study of the systematics in the ω analysis are presented in Table 4. The largest contribution comes from the uncertainty in the width of the signal. The value assigned is the result of varying the width by $\pm 10\%$. The uncertainty in π^0 efficiency also yields a large contribution to the overall systematic error.

The extrapolation of the differential cross section from $x_p = 0.05$ to $x_p = 0$ introduces an additional systematic uncertainty. The measured multiplicity is scaled using the JETSET 7.4 to calculate the missing fraction ($\approx 40\%$), JETSET 7.4 is used as this describes the measured ϕ and K^{*0} distribution at low x_p much better than JETSET 7.3 and HERWIG 5.6. The uncertainty in the scaling is taken as the largest difference between the Monte Carlos.

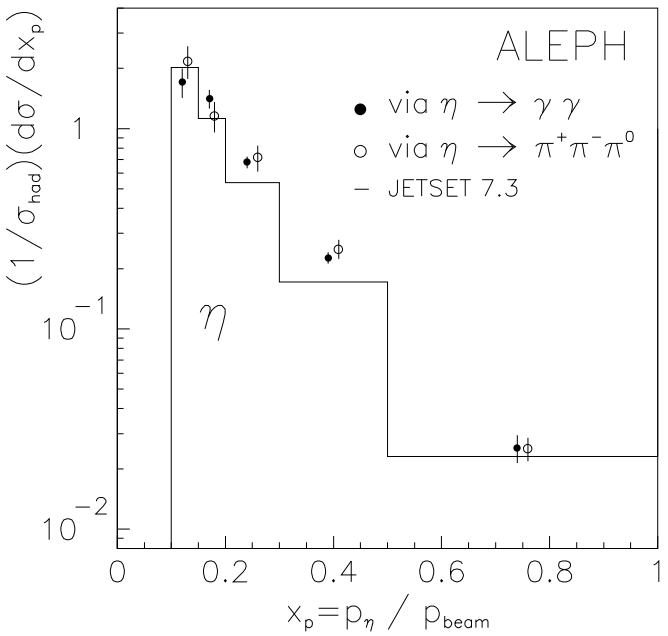

Figure 9: *The η fragmentation function extracted in the channel $\eta \rightarrow \pi^+\pi^-\pi^0$ is compared to that measured previously by ALEPH in the channel $\eta \rightarrow \gamma\gamma$. For $x_p > 0.1$ the average multiplicity of $0.301 \pm 0.019 \pm 0.035$ measured in this analysis is consistent with the previous measurement of $0.282 \pm 0.015 \pm 0.016$ [21]. (The open and solid circles are displaced horizontally so they do not overlap.)*

As a check of the efficiency, the fitting procedure was repeated for the η and the results compared with a previous measurement by ALEPH [21] in the channel $\eta \rightarrow \gamma\gamma$. For both analyses, signals are extracted for $x_p > 0.10$. The previous measurements have been rebinned for direct comparison. From Figure 9, it can be seen that the two analyses give consistent results for the fragmentation function and the mean η multiplicity.

4.2.3 Systematic errors for the $K^{*0}(892)$

Systematic uncertainties (see Table 6) from event and track selection and particle identification are investigated by varying the cuts. The fit range was varied by $\pm 40\,\mathrm{MeV}/c^2$. Uncertainties in $\mathrm{d}E/\mathrm{d}x$ were studied as well as changes in the shape of the resonances (e.g., changing the width of the K^{*0} by $5\,\mathrm{MeV}/c^2$ or switching the Bose-Einstein effect off for the ρ^0 shape) and background, where other parameterizations have been used. Uncertainties from reflections come mainly from the limited knowledge of the ω and ρ rate. They were varied by $+10\%$ and -30%. Monte Carlo studies were used to check how well the fitting method reproduces the number of K^{*0}'s. Unfortunately a different signal function must be used, as the Monte Carlo uses a non-relativistic Breit-Wigner generated in a limited mass range. The differences of reconstructed and fitted K^{*0} in the simulation are taken as systematic uncertainties.

4.2.4 Systematic errors for the $\phi(1020)$

Table 8 lists the errors on the ϕ rate. Of importance is the limited knowledge of the detector resolution. Γ_{res} must be taken from Monte Carlo studies and is varied by 20% and 10% for $x_p < 0.1$ and $x_p \geq 0.1$. The uncertainties from the track and event selection are found to be important only for low x_p.

The influence of the background parameterization is obtained by replacing the exponential by a polynomial function. Monte Carlo studies were used to check how well the fitting method reproduces the number of ϕ's. The differences of reconstructed and fitted ϕ in the simulation are taken as systematic uncertainties.

Other contributions such as changing the fit range and uncertainty of the branching fraction $\phi \to K^+K^-$ are found to be small.

4.3 Strangeness suppression

For the determination of the strangeness suppression, the assumption is made that the relative production of non-strange and strange vector mesons is governed by the frequency by which an up or down quark is replaced by a strange quark. The up and down quark, being equally produced, the ratios $N(K^{*0})/2N(\rho^0)$, $N(K^{*0})/2N(\omega)$, and $2N(\phi)/N(K^{*0})$ therefore should represent $N(\mathrm{s})/N(\mathrm{u})$; the latter ratio is usually abbreviated s/u. The ratios are expected to agree only when corrected for decays and leading quarks. It is, however, not obvious whether one should correct for decays from higher spin states such as tensor mesons.

Without any correction, the results for s/u from the measured vector meson rates are: $N(K^{*0})/2N(\rho^0) = 0.29 \pm 0.01 \pm 0.05$, $N(K^{*0})/2N(\omega) = 0.39 \pm 0.02 \pm 0.06$, and $2N(\phi)/N(K^{*0}) = 0.29 \pm 0.01 \pm 0.04$. This compares well with the values 0.36, 0.38, and 0.34 for JETSET 7.3, respectively, where the parameter for the strangeness suppression was at its default value 0.3.

4.4 Ratio of Vector Mesons to Pseudoscalar Mesons

A comparison of the inclusive spectra of vector and pseudoscalar mesons provides information about the relative probabilities for the corresponding spin states to be produced in the hadronization.

In JETSET 7.3 the probability to produce a strange meson with spin 1 is controlled by the parameter $[\mathrm{V}/(\mathrm{V}+\mathrm{P})]_\mathrm{s}$, with a default value of 0.6. This ratio pertains to mesons directly produced in the hadronization, and leads to a predicted ratio of vector to vector plus pseudoscalar kaons of $N(\mathrm{K}^{*0})/(N(\mathrm{K}^{*0}) + N(\mathrm{K}^0)) = 0.33$. (The multiplicity ratio cannot be directly compared with the parameter of $[\mathrm{V}/(\mathrm{V}+\mathrm{P})]_\mathrm{s}$ since 12% of the K^{*0} and 66% of the K^0 mesons come from decays.) Using the previously published number of K^0's [22] a measured value of $N(\mathrm{K}^{*0})/(N(\mathrm{K}^{*0}) + N(\mathrm{K}^0)) = 0.29 \pm 0.02$ is obtained.

4.5 Cross section as function of ξ_p

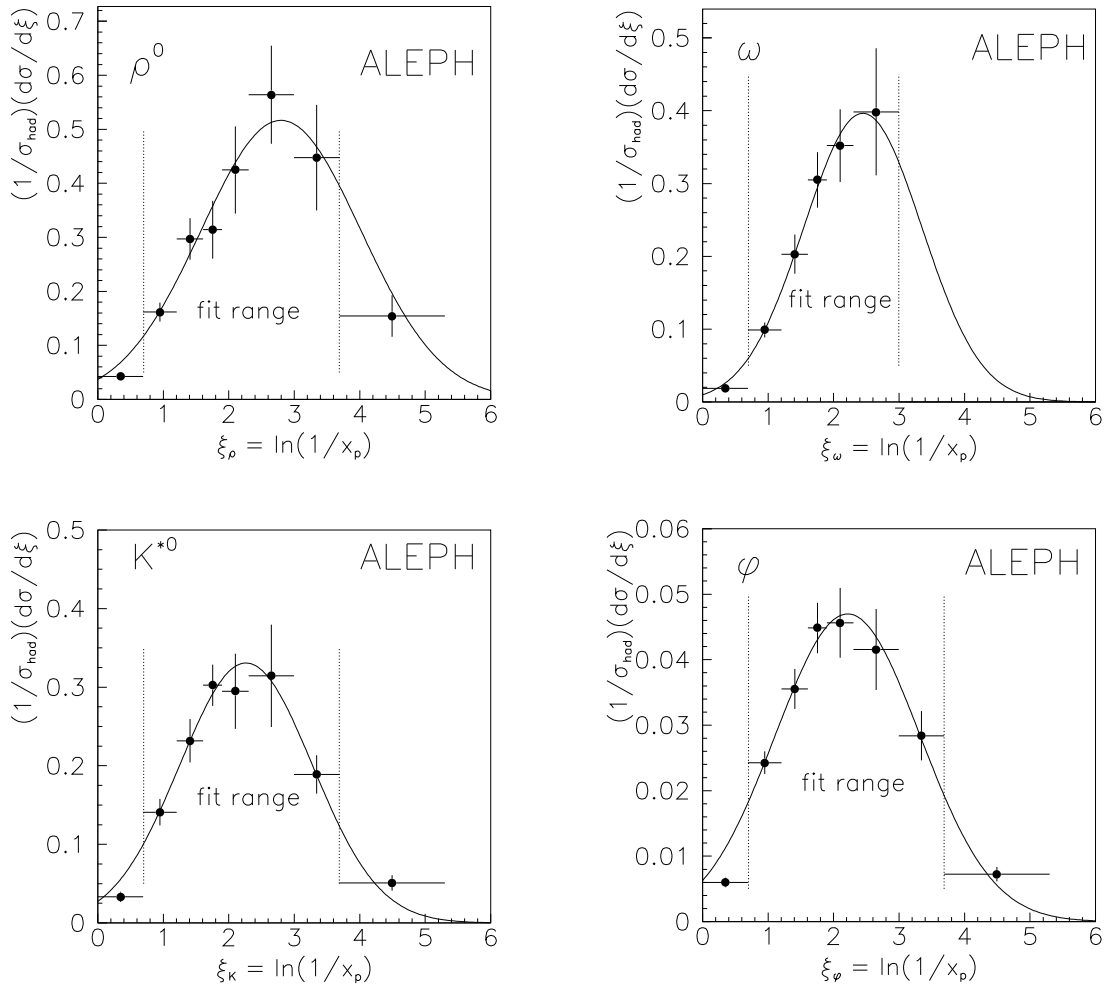

Figure 10: *Differential cross section for ρ^0, ω, K^{*0}, and ϕ as a function of ξ_p. The spectra are fitted with a Gaussian over the range indicated by the dotted lines.*

In the Figures 10, the inclusive cross sections for the vector mesons are given as a function of $\xi_p = \ln(1/x_p)$. The modified leading logarithm approximation combined with the local parton-hadron duality model [23] predicts that the position of the maximum should depend on the particle mass. This position may be modified by heavy flavour decays; vector mesons, however, are expected to be predominantly produced by the fragmentation. The maxima follow the expected behaviour, i.e., the momentum spectrum is harder for particles with higher masses. The position of the maximum is obtained by fitting a Gaussian in the range $0.69 < \xi_p < 3.7$. The maxima are at $\xi_p^{\max} = 2.80 \pm 0.19$ for $\rho^0(770)$, 2.26 ± 0.05 for $\mathrm{K}^{*0}(892)$, and 2.21 ± 0.03 for $\phi(1020)$. The maximum for the $\omega(782)$ lies too close to the edge of the fit range ($0.69 < \xi_p < 3.0$) for a reliable value to be given.

5 Conclusion

The inclusive production of $\rho^0(770)$, $\omega(782)$, $\mathrm{K}^{*0}(892)$, and $\phi(1020)$ in hadronic Z decays has been studied and compared to model predictions. The total multiplicities are collected in Table 9 and compared to other measurements at LEP. Predictions from the models JETSET 7.3, JETSET 7.4, and HERWIG 5.6 are also given.

The agreement between data and JETSET in the vector meson momentum spectra is substantially improved by including a simulation of tensor meson production in JETSET 7.4 and also by using improved decay tables.

The inclusion of Bose-Einstein correlations in the Monte Carlo was found to be important for a good description of the two-pion invariant mass spectrum of both like-sign and unlike-sign pairs. A fair description for the like-sign subtracted mass spectrum of the data was obtained with JETSET, when Bose-Einstein correlations are enabled.

The ρ^0 meson is found to have an average multiplicity per event of $1.453 \pm 0.065(\mathrm{stat}) \pm 0.201(\mathrm{syst})$. The momentum spectrum and the total rate agree with tuned JETSET (1.46 ρ^0 per event). The HERWIG 5.6 prediction is lower (1.31), but still in agreement with the data. The measured ρ^0 line shape is distorted and the mass appears shifted. In the framework of the JETSET model, this is attributed to Bose-Einstein correlations. The change in phase space for identical pions also alters the particle correlations for unlike-sign pion pairs, i.e., it influences the background and the ρ^0 line shape. Therefore a correct description of the Bose-Einstein effect is needed to extract useful information. Using JETSET, an adequate description of the data was obtained by using a chaoticity parameter $\lambda = 2.1$; a small correction in Q was added as well.

The average multiplicity per event for the ω has been measured for $x_p > 0.05$ to be $0.637 \pm 0.034(\mathrm{stat}) \pm 0.074(\mathrm{syst})$. An extrapolation of this multiplicity to $x_p = 0$ yields $1.066 \pm 0.058(\mathrm{stat}) \pm 0.124(\mathrm{syst}) \pm 0.044(\mathrm{scale})$ per event. The multiplicity lies between the prediction of JETSET 7.3 (1.37 ω per event) and HERWIG 5.6 (0.80 ω per event). The agreement improves slightly when tensor production is included in the Monte Carlo JETSET 7.4 (1.23 ω per event).

The rate of ω production is expected to be almost the same as for the ρ^0 since the two have essentially the same flavour content, the same spin, and nearly the same mass, only

differing in isospin. The ratio of the measured production rate of the ρ^0 to that of the ω is 1.36 ± 0.27. This agrees within errors with the value of 1.07 from JETSET 7.3, which does not distinguish isospin states. Therefore no evidence for isospin dependence is seen.

The average multiplicity per event of the K^{*0} is $0.830 \pm 0.015(\text{stat}) \pm 0.088(\text{syst})$, in agreement with measurements from other LEP experiments. The momentum spectrum is fairly well described by the models JETSET 7.3 and HERWIG. The total rate is between the rates from JETSET 7.3 and HERWIG, but compatible with both models. The agreement is excellent using JETSET 7.4 when the tensor production is included, in particular at low x_p (< 0.05), where the K^{*0} is suppressed compared to JETSET 7.3 and HERWIG.

The average ϕ multiplicity per event has been measured to be $0.122 \pm 0.004(\text{stat}) \pm 0.008(\text{syst})$. This result agrees with the prediction of HERWIG, whereas JETSET 7.3 over-predicts by about 50%. The momentum dependence of the ϕ production is best reproduced by including tensor production in JETSET 7.4: as for the K^{*0}, the improvement is especially notable at low x_p.

Acknowledgements
It is a pleasure to thank the technical personnel of the collaborating institutions for their support in constructing and maintaining the ALEPH experiment. Those of the collaboration not from member states thank CERN for its hospitality.

References

[1] D. Buskulic et al. (ALEPH Collab.), Z. Phys. C55 (1992), 209.

[2] T. Sjöstrand, Comp. Phys. Comm. 27 (1982) 243;
T. Sjöstrand, Comp. Phys. Comm. 28 (1983) 229;
T. Sjöstrand and M. Bengtsson, Comp. Phys. Comm. 43 (1987) 367.

[3] W. Hofmann, Ann. Rev. Nucl. and Part. Sci. 38 (1988) 279.

[4] M. Aguilar-Benitez et al. (Particle Data Group), Phys. Rev. D45 (1992) 1;
M. Aguilar-Benitez et al. (Particle Data Group), Phys. Rev. D50 (1994) 1175.

[5] G. Goldhaber et al., Phys. Rev. 120 (1960) 300.

[6] P. Abreu et al. (DELPHI Collab.), Phys. Lett. B298 (1993) 236.

[7] P. Abreu et al. (DELPHI Collab.), Z. Phys. C65 (1995) 587.

[8] R. Akers et al. (OPAL Collab.), CERN-PPE/95-027 (1995) submitted to Z. Phys. C.

[9] D. Decamp et al. (ALEPH Collab.), Nucl. Instr. Meth. A294 (1990) 121;
D. Buskulic et al. (ALEPH Collab.), Nucl. Instr. Meth. A360 (1995) 481.

[10] D. Decamp et al. (ALEPH Collab.), Z. Phys. C53 (1992), 1.

[11] J.E. Campagne and R. Zitoun, Z. Phys. C43 (1989) 469.

[12] D. Buskulic et al. (ALEPH Collab.), Phys. Lett. B292 (1992) 210.

[13] G. Marchesini and B.R. Webber, Nucl. Phys. B310 (1988) 461;
G. Marchesini et al., Comp. Phys. Comm. 67 (1992) 465.

[14] J.D. Jackson, Nuovo Cimento 34 (1964) 1644.

[15] R.J. Apsimon et al. (OMEGA Collab.), Z. Phys. C53 (1992) 581.

[16] G.D. Lafferty, Z. Phys. C60 (1993) 659.

[17] S. Haywood, RAL-94-074 (1994).

[18] P.D. Acton et al. (OPAL Collab.), Z. Phys. C56 (1992) 521.

[19] P. Abreu et al. (DELPHI Collab.), Z. Phys. C63 (1994) 17.

[20] P.D. Acton et al. (OPAL Collab.), Phys. Lett. B267 (1991) 143;
D. Decamp et al. (ALEPH Collab.), Z. Phys. C54 (1992) 75;
P. Abreu et al. (DELPHI Collab.), Phys. Lett. B286 (1992) 201.

[21] S. Haywood (ALEPH Collab.), Presented at the 27th International Conference on High Energy Physics, Glasgow (July 1994).

[22] D. Buskulic et al. (ALEPH Collab.), Z. Phys. C64 (1994) 361.

[23] Y.I. Azimov, Yu.L. Dokshitzer, V.A. Khoze, and S.I. Troyan, Z. Phys. C27 (1985) 65;
Y.I. Azimov, Yu.L. Dokshitzer, V.A. Khoze, and S.I. Troyan, Z. Phys. C31 (1986) 213.

x_p *range*	χ^2/dof	*Multiplicity* $\rho^0(770)$/Z *decay*	$1/\sigma_{had} d\sigma/dx_p$
0.005-0.025	56/59	0.248 ± 0.041 ± 0.047	12.42 ± 2.04 ± 2.33
0.025-0.05	57/59	0.310 ± 0.033 ± 0.059	12.41 ± 1.33 ± 2.36
0.05 -0.10	84/59	0.391 ± 0.029 ± 0.056	7.82 ± 0.58 ± 1.11
0.10 -0.15	61/59	0.172 ± 0.018 ± 0.027	3.44 ± 0.36 ± 0.55
0.15 -0.20	52/59	0.090 ± 0.010 ± 0.012	1.81 ± 0.20 ± 0.24
0.20 -0.30	87/59	0.120 ± 0.010 ± 0.012	1.20 ± 0.10 ± 0.12
0.30 -0.50	65/59	0.083 ± 0.005 ± 0.007	0.41 ± 0.03 ± 0.04
0.50 -1.00	49/59	0.030 ± 0.002 ± 0.003	0.059 ± 0.004 ± 0.005
0.005-1.00		1.445 ± 0.065 ± 0.200	
all x_p		1.453 ± 0.065 ± 0.201	

Table 1: *Measured multiplicities and differential cross sections for* ρ^0. *The results of summing over the measured* x_p *intervals are also given, including extrapolation to the full* x_p *range.*

Source of error	x_p *interval*								
	all x_p	1	2	3	4	5	6	7	8
K^{*0}; ω; f_0	11.1	11.4	15.6	12.7	12.4	5.0	7.7	3.0	3.4
dE/dx	5.1	7.2	5.4	1.8	8.7	11.2	3.3	6.1	1.7
$\Delta\Gamma_0$, Δm	4.5	5.6	4.9	5.7	3.7	2.0	4.4	3.2	3.2
Fit range	0.9	2.4	6.4	1.8	1.8	3.4	3.2	2.1	0.6
Trk./ev. selection	4.5	11.6	4.9	1.6	2.2	2.4	2.5	4.1	6.9
Systematic error (quadrature total)	13.8	18.8	19.0	14.2	15.9	13.1	10.3	8.8	8.5
Statistical error	4.5	16.5	10.7	7.4	10.4	10.9	7.9	6.5	7.2
Total error	14.5	25.0	21.8	16.1	19.0	17.1	13.0	10.9	11.1

Table 2: *Systematic and statistical errors for* ρ^0. *All values are expressed in* %.

x_p *range*	χ^2/dof	*Multiplicity* $\omega(782)$/Z *decay*	$1/\sigma_{had}d\sigma/dx_p$
0.005-0.025			
0.025-0.05			
0.05-0.10	97/68	$0.2656 \pm 0.0313 \pm 0.0489$	$5.312 \pm 0.627 \pm 0.977$
0.10-0.15	114/72	$0.1409 \pm 0.0111 \pm 0.0166$	$2.817 \pm 0.223 \pm 0.332$
0.15-0.20	74/72	$0.0871 \pm 0.0059 \pm 0.0091$	$1.743 \pm 0.118 \pm 0.183$
0.20-0.30	80/72	$0.0812 \pm 0.0044 \pm 0.0098$	$0.812 \pm 0.044 \pm 0.098$
0.30-0.50	97/72	$0.0494 \pm 0.0023 \pm 0.0046$	$0.247 \pm 0.012 \pm 0.023$
0.50-1.00	69/72	$0.0126 \pm 0.0009 \pm 0.0014$	$0.025 \pm 0.002 \pm 0.003$
0.050-1.00		$0.637 \pm 0.034 \pm 0.074$	
all x_p		$1.066 \pm 0.058 \pm 0.124 \pm 0.044$	

Table 3: *Measured multiplicities and differential cross sections for* ω*. The results of summing over the measured* x_p *intervals are also given, including the extrapolation to the full* x_p *range with an additional error due to the uncertainty in the extrapolation.*

Source of error	x_p *interval*								
	all x_p	1	2	3	4	5	6	7	8
Event selection	3.9	-	-	9.5	1.0	2.3	2.6	2.0	1.4
Charged trk. selection	2.3	-	-	3.6	3.3	2.6	2.1	1.8	2.4
E_γ *energy*	3.4	-	-	10.3	3.0	3.0	2.3	1.9	0.8
π^0 *window*	2.2	-	-	3.7	3.4	4.7	5.8	1.1	2.2
π^0 *efficiency*	5.6	-	-	6.7	5.8	4.2	4.2	4.4	7.1
Fit range	4.5	-	-	5.8	4.6	2.4	2.9	3.3	3.3
Signal width	6.8	-	-	6.1	7.2	6.6	8.4	6.6	7.0
Systematic error (quadrature total)	11.6	-	-	18.4	11.8	10.5	12.1	9.3	11.1
Statistical error	5.4	-	-	11.8	7.9	6.8	5.4	4.7	7.0
Total error	12.8	-	-	21.9	14.2	12.5	13.3	10.4	13.1

Table 4: *Systematic and statistical errors for* ω*. All values are expressed in* %*.*

x_p *range*	χ^2/dof	*Multiplicity* $K^{*0}(892)/Z$ *decay*	$1/\sigma_{had}d\sigma/dx_p$
0.005-0.025	99/65	0.082 ± 0.0072 ± 0.014	4.10 ± 0.36 ± 0.71
0.025-0.05	76/65	0.131 ± 0.0073 ± 0.016	5.24 ± 0.29 ± 0.61
0.05 -0.10	120/65	0.218 ± 0.0073 ± 0.044	4.36 ± 0.15 ± 0.89
0.10 -0.15	55/65	0.119 ± 0.0066 ± 0.018	2.39 ± 0.13 ± 0.36
0.15 -0.20	62/65	0.087 ± 0.0037 ± 0.007	1.74 ± 0.07 ± 0.15
0.20 -0.30	89/65	0.094 ± 0.0036 ± 0.010	0.94 ± 0.04 ± 0.11
0.30 -0.50	75/65	0.073 ± 0.0028 ± 0.0082	0.36 ± 0.01 ± 0.043
0.50 -1.00	56/65	0.023 ± 0.0011 ± 0.0044	0.046 ± 0.002 ± 0.009
0.005-1.00		0.827 ± 0.015 ± 0.088	
all x_p		0.830 ± 0.015 ± 0.088	

Table 5: *Measured multiplicities and differential cross sections for* K^{*0}. *The results of summing over the measured* x_p *intervals are also given, including extrapolation to the full* x_p *range.*

Source of error	x_p *interval*								
	all x_p	1	2	3	4	5	6	7	8
Trk./ev. selection	4.6	8.2	8.6	9.4	6.8	2.6	3.5	1.0	5.0
$\mathrm{d}E/\mathrm{d}x$	3.6	3.9	1.4	2.4	10.6	2.1	7.4	1.8	12.1
Fit range	0.3	2.5	0.9	1.6	0.3	0.4	0.8	0.7	0.9
Background	3.1	5.3	2.9	10.4	2.6	0.8	0.9	2.8	0.7
ρ^0 *shape*	4.7	9.3	4.4	8.2	3.3	2.0	2.9	2.0	9.3
ρ^0, ω *rate*	1.0	4.7	0.8	4.6	1.2	1.2	0.1	0.1	1.3
K^{*0} *shape*	6.7	8.5	5.2	7.7	6.5	6.3	6.4	5.9	5.6
Fitting method	0.7	1.8	1.7	7.9	3.6	0.0	3.0	8.6	8.0
Systematic error (quadrature total)	10.6	17.3	11.6	20.4	15.2	7.6	11.3	11.2	18.8
Statistical error	1.9	8.8	5.6	3.4	5.5	4.3	3.8	3.8	4.9
Total error	10.8	19.5	12.9	20.7	16.2	8.7	11.9	11.8	19.4

Table 6: *Systematic and statistical errors for* K^{*0}. *All values are expressed in* %.

x_p *range*	χ^2/dof	*Multiplicity* $\phi(1020)$/Z *decay*	$1/\sigma_{had}d\sigma/dx_p$
$0.005-0.025$	$72/61$	$0.01167 \pm 0.0011 \pm 0.0014$	$0.584 \pm 0.055 \pm 0.069$
$0.025-0.05$	$107/76$	$0.01967 \pm 0.0022 \pm 0.0014$	$0.787 \pm 0.089 \pm 0.056$
$0.05-0.10$	$96/76$	$0.02882 \pm 0.0023 \pm 0.0036$	$0.576 \pm 0.046 \pm 0.073$
$0.10-0.15$	$195/159$	$0.01848 \pm 0.0013 \pm 0.0017$	$0.370 \pm 0.026 \pm 0.035$
$0.15-0.20$	$148/159$	$0.01288 \pm 0.00095 \pm 0.00055$	$0.258 \pm 0.019 \pm 0.011$
$0.20-0.30$	$185/159$	$0.01440 \pm 0.00089 \pm 0.00085$	$0.144 \pm 0.0089 \pm 0.0085$
$0.30-0.50$	$140/159$	$0.01240 \pm 0.00065 \pm 0.00060$	$0.0620 \pm 0.0033 \pm 0.0030$
$0.50-1.00$	$191/159$	$0.00415 \pm 0.00028 \pm 0.00037$	$0.00831 \pm 0.00057 \pm 0.00074$
$0.005-1.00$		$0.122 \pm 0.004 \pm 0.008$	
all x_p		$0.122 \pm 0.004 \pm 0.008$	

Table 7: *Measured multiplicities and differential cross sections for* ϕ*. The results of summing over the measured* x_p *intervals are also given, including extrapolation to the full* x_p *range.*

Source of error	x_p *interval*								
	all x_p	1	2	3	4	5	6	7	8
Trk./ev. selection	1.4	4.7	3.0	2.5	–	–	–	–	–
$\mathrm{d}E/\mathrm{d}x$	2.3	2.7	0.5	8.3	–	–	–	–	–
Generator dependence	2.1	8.0	0.2	2.4	0.6	1.2	1.3	2.5	2.5
$\Delta\Gamma_{\mathrm{res}}$	2.4	5.8	2.7	2.4	0.9	1.6	1.8	1.8	3.0
$\Delta\Gamma_0$	1.5	1.7	1.7	2.0	0.7	1.3	1.7	1.1	1.0
Background	3.3	2.8	5.2	8.2	4.9	1.4	1.0	1.0	0.5
Fitting method	1.2	–	–	–	2.7	2.7	4.7	2.8	7.0
Fit range	1.1	1.0	1.0	1.0	1.0	1.0	1.0	1.0	3.3
Branching ratio	1.6	1.6	1.6	1.6	1.6	1.6	1.6	1.6	1.6
Systematic error (quadrature total)	6.1	11.9	7.1	12.6	9.4	4.3	5.9	4.8	8.9
Statistical error	3.2	9.4	11.2	8.0	7.0	7.4	6.2	5.2	6.7
Total error	6.9	15.2	13.3	14.9	11.7	8.6	8.6	7.1	11.1

Table 8: *Systematic and statistical errors for* ϕ*. All values are expressed in* %*.*

Meson	*Experiment*	*Multiplicity*	JETSET 7.3	JETSET 7.4	HERWIG 5.6
ρ^0	ALEPH DELPHI	1.45 ± 0.21 1.21 ± 0.15	1.46	1.45	1.31
ω	ALEPH	1.07 ± 0.14	1.37	1.23	0.80
K^{*0}	ALEPH DELPHI OPAL	0.83 ± 0.09 0.97 ± 0.36 0.74 ± 0.04	1.05	0.78	0.79
ϕ	ALEPH OPAL	0.122 ± 0.009 0.100 ± 0.008	0.180	0.129	0.123

Table 9: *Measured multiplicities for vector mesons. The rates as measured by the LEP experiments in comparison to ALEPH tuned model predictions.* JETSET 7.4 *includes tensor production.*